Characterization of holographically generated beams via phase retrieval based on Wigner distribution projections

José A. Rodrigo,[1,*] Tatiana Alieva,[2] Alejandro Cámara,[2] Ó. Martínez-Matos,[2] Pavel Cheben,[3] and María L. Calvo,[2]

[1]*Instituto de Óptica, CSIC, Serrano 121, 28006 Madrid, Spain*
[2]*Universidad Complutense de Madrid, Facultad de Ciencias Físicas, Ciudad Universitaria s/n, 28040 Madrid, Spain*
[3]*Institute for Microstructural Sciences, National Research Council of Canada, KlA OR6 Ottawa, Canada*
[*]*jose.a.rodrigo@optica.csic.es*

Abstract: In this work, we propose a robust and versatile approach for the characterization of the complex field amplitude of holographically generated coherent-scalar paraxial beams. For this purpose we apply an iterative algorithm that allows recovering the phase of the generated beam from the measurement of its Wigner distribution projections. Its performance is analyzed for beams of different symmetry: Laguerre-Gaussian, Hermite-Gaussian and spiral ones, which are obtained experimentally by a computer generated hologram (CGH) implemented on a programmable spatial light modulator (SLM). Using the same method we also study the quality of their holographic recording on a highly efficient photopolymerizable glass. The proposed approach is useful for the creation of adaptive CGH that takes into account the peculiarities of the SLM, as well as for the quality control of the holographic data storage.

OCIS codes: (140.3300) Laser beam shaping; (090.1760) Computer holography; (090.7330) Holography: Volume gratings; (070.2590) Fourier optics and signal processing: ABCD transforms.

References

1. A. E. Siegman, *Lasers* (University Science Books, 1986).
2. F. M. Dickey, S. C. Holswade, and D. L. Shealy, eds., *Laser Beam Shaping Applications* (CRC Press, 2005).
3. A. Ashkin, *Optical Trapping and Manipulation of Neutral Particles Using Lasers: A Reprint Volume With Commentaries* (World Scientific Publishing Company, 2006).
4. J. P. Kirk and A. L. Jones, "Phase-only complex-valued spatial filter," J. Opt. Soc. Am. **61**, 1023–1028 (1971).
5. J. A. Davis, D. M. Cottrell, J. Campos, M. J. Yzuel, and I. Moreno, "Encoding amplitude information onto phase-only filters," Appl. Opt. **38**, 5004–5013 (1999).
6. V. Arrizón, U. Ruiz, R. Carrada, and L. A. González, "Pixelated phase computer holograms for the accurate encoding of scalar complex fields," J. Opt. Soc. Am. A **24**, 3500–3507 (2007).
7. B. Hennelly, J. Ojeda-Castañeda, and M. Testorf, eds., *Phase Space Optics: Fundamentals and Applications* (McGraw-Hill, 2009).
8. T. Alieva and J. A. Rodrigo, "Iterative phase retrieval from Wigner Distribution Projections," in "Signal Recovery and Synthesis," (Optical Society of America, 2009), p. STuD2.
9. A. Cámara, T. Alieva, J. A. Rodrigo, and M. L. Calvo, "Phase space tomography reconstruction of the Wigner distribution for optical beams separable in Cartesian coordinates," J. Opt. Soc. Am. A **26**, 1301–1306 (2009).
10. M. Born and E. Wolf, *Principles of Optics* (Cambridge University Press, Cambridge, 1999).

#140087 - $15.00 USD Received 22 Dec 2010; revised 20 Feb 2011; accepted 23 Feb 2011; published 17 Mar 2011

11. J. Otón, P. Ambs, M. S. Millán, and E. Pérez-Cabré, "Multipoint phase calibration for improved compensation of inherent wavefront distortion in parallel aligned liquid crystal on silicon displays," Appl. Opt. **46**, 5667–5679 (2007).
12. J. D. Schmidt, M. E. Goda, and B. D. Duncan, "Aberration production using a high-resolution liquid-crystal spatial light modulator," Appl. Opt. **46**, 2423–2433 (2007).
13. A. Jesacher, A. Schwaighofer, S. Fürhapter, C. Maurer, S. Bernet, and M. Ritsch-Marte, "Wavefront correction of spatial light modulators using an optical vortex image," Opt. Express **15**, 5801–5808 (2007).
14. C. López-Quesada, J. Andilla, and E. Martín-Badosa, "Correction of aberration in holographic optical tweezers using a Shack-Hartmann sensor," Appl. Opt. **48**, 1084–1090 (2009).
15. L. Paterson, M. P. MacDonald, J. Arlt, W. Sibbett, P. E. Bryant, and K. Dholakia, "Controlled rotation of optically trapped microscopic particles," Science **292**, 912–914 (2001).
16. A. Mair, A. Vaziri, G. Weihs, and A. Zeilinger, "Entanglement of the orbital angular momentum states of photons," Nature **412**, 313–316 (2001).
17. G. Molina-Terriza, J. P. Torres, and L. Torner, "Twisted photons," Nat. Phys. **3**, 305–310 (2007).
18. Y. Y. Schechner, R. Piestun, and J. Shamir, "Wave propagation with rotating intensity distributions," Phys. Rev. E **54**, R50–R53 (1996).
19. E. G. Abramochkin and V. G. Volostnikov, "Spiral light beams," Sov. Phys. Usp. **47**, 1177 (2004).
20. T. Alieva, E. Abramochkin, A. Asenjo-Garcia, and E. Razueva, "Rotating beams in isotropic optical system," Opt. Express **18**, 3568–3573 (2010).
21. J. P. Guigay, "Fourier-transform analysis of Fresnel diffraction patterns and in-line holograms," Optik **49**, 121–125 (1977).
22. M. R. Teague, "Deterministic phase retrieval: a Green's function solution," J. Opt. Soc. Am. **73**, 1434–1441 (1983).
23. T. E. Gureyev and K. A. Nugent, "Rapid quantitative phase imaging using the transport of intensity equation," Opt. Commun. **133**, 339–346 (1997).
24. U. Gopinathan, G. Situ, T. J. Naughton, and J. T. Sheridan, "Noninterferometric phase retrieval using a fractional Fourier system," J. Opt. Soc. Am. A **25**, 108–115 (2008).
25. R. W. Gerchberg and W. O. Saxton, "A practical algorithm for the determination of phase from image and diffraction plane pictures," Optik **35**, 237–246 (1972).
26. Z. Zalevsky, D. Mendlovic, and R. G. Dorsch, "Gerchberg-Saxton algorithm applied in the fractional Fourier or the Fresnel domain," Opt. Lett. **21**, 842–844 (1996).
27. M. Nieto-Vesperinas, R. Navarro, and F. J. Fuentes, "Performance of a simulated-annealing algorithm for phase retrieval," J. Opt. Soc. Am. A **5**, 30–38 (1988).
28. J. A. Rodrigo, H. Duadi, T. Alieva, and Z. Zalevsky, "Multi-stage phase retrieval algorithm based upon the gyrator transform," Opt. Express **18**, 1510–1520 (2010).
29. D. Mendlovic, Z. Zalevsky, and N. Konforti, "Computation considerations and fast algorithms for calculating the diffraction integral," J. Mod. Opt. **44**, 407 (1997).
30. J. B. Bentley, J. A. Davis, M. A. Bandres, and J. C. Gutiérrez-Vega, "Generation of helical Ince-Gaussian beams with a liquid-crystal display," Opt. Lett. **31**, 649–651 (2006).
31. N. Matsumoto, T. Ando, T. Inoue, Y. Ohtake, N. Fukuchi, and T. Hara, "Generation of high-quality higher-order Laguerre-Gaussian beams using liquid-crystal-on-silicon spatial light modulators," J. Opt. Soc. Am. A **25**, 1642–1651 (2008).
32. T. Ando, Y. Ohtake, N. Matsumoto, T. Inoue, and N. Fukuchi, "Mode purities of Laguerre–Gaussian beams generated via complex-amplitude modulation using phase-only spatial light modulators," Opt. Lett. **34**, 34–36 (2009).
33. A. Lizana, A. Márquez, L. Lobato, Y. Rodange, I. Moreno, C. Iemmi, and J. Campos, "The minimum euclidean distance principle applied to improve the modulation diffraction efficiency in digitally controlled spatial light modulators," Opt. Express **18**, 10581–10593 (2010).
34. I. Moreno, A. Lizana, A. Márquez, C. Iemmi, E. Fernández, J. Campos, and M. J. Yzuel, "Time fluctuations of the phase modulation in a liquid crystal on silicon display: characterization and effects in diffractive optics," Opt. Express **16**, 16711–16722 (2008).
35. R. J. Noll, "Zernike polynomials and atmospheric turbulence," J. Opt. Soc. Am. **66**, 207–211 (1976).
36. V. Arrizón, G. Méndez, and D. S. de La-Llave, "Accurate encoding of arbitrary complex fields with amplitude-only liquid crystal spatial light modulators," Opt. Express **13**, 7913–7927 (2005).
37. J. Arlt, K. Dholakia, L. Allen, and M. J. Padgett, "The production of multiringed Laguerre-Gaussian modes by computer-generated holograms," J. Mod. Opt. **45**, 231–1237 (1998).
38. F. del Monte, O. Martínez, J. Rodrigo, M. Calvo, and P. Cheben, "A volume holographic sol-gel material with large enhancement of dynamic range by incorporation of high refractive index species," Adv. Mater. **18**, 2014–2017 (2006).
39. O. Martínez-Matos, J. A. Rodrigo, M. P. Hernández-Garay, J. G. Izquierdo, R. Weigand, M. L. Calvo, P. Cheben, P. Vaveliuk, and L. Bañares, "Generation of femtosecond paraxial beams with arbitrary spatial distribution," Opt. Lett. **35**, 652–654 (2010).

#140087 - $15.00 USD Received 22 Dec 2010; revised 20 Feb 2011; accepted 23 Feb 2011; published 17 Mar 2011

1. Introduction

Generation of laser beams with a determined amplitude and phase distribution is a relevant challenge in optics. Holography has demonstrated to be a powerful tool for this task. In particular, computer-generated holograms (CGHs) result very useful in applications where a dynamic beam synthesis is demanded as for example laser beam shaping [1, 2], optical micro-particle manipulation [3], etc. The CGHs are often addressed onto programmable spatial light modulators (SLMs) based on the liquid crystal on silicon (LCoS) display technology, which provide versatile beam control almost in real time. During the last decades various methods for encoding of the complex field onto phase-only CGHs have been developed [4]−[6]. However, the wavefront distortion arising from flatness deviation of the SLM, moderate-low spatial resolution and limited phase depth yield the deviation of the generated beam from the programmed one. To characterize and evaluate the quality of the holographic beam synthesis usually only the intensity beam distribution is taken into account. Nevertheless, for entire characterization of the coherent scalar beam the information about its phase is required. Here we propose a beam characterization technique which includes its phase recovery from the Wigner distribution (WD) projections that coincide with the intensity distributions measured at the output of the proper optical system, see [7]−[9]. This approach is not interferometric and can be experimentally realized by a robust optical setup. Notice that the knowledge of the phase distribution allows verifying the global beam quality generation. Moreover, the decomposition of the retrieved phase on terms of Zernike polynomials [10] provides a diagnostics of the wavefront distortion in the generated beam.

The proposed phase retrieval technique can also be used as an alternative to the methods reported in the references [11]−[14] and the ones cited therein, for estimation of the non-desirable wavefront distortion introduced by the optical system including the SLM display. To compensate such deviations the CGH has to be modified leading to an adaptive CGH (ACGH). We experimentally demonstrate the advantage of using the ACGHs for high quality beam synthesis.

This paper is organized as it follows. Section 2 reviews the multireference iterative phase retrieval approach, which is the main tool of the proposed technique for optical setup and beam characterization. In section 3 we first remind two main phase-only CGH encoding methods for arbitrary complex scalar-field generation. Then we apply the phase retrieval technique for the analysis of the optical setup further used for holographic beam generation. The wavefront distortions are analyzed and taken into account for the creation of the ACGHs. The beams obtained from the ACGHs, for both encoding methods, are compared using the proposed characterization technique. As examples we have chosen several beams with different symmetries such as Laguerre-Gaussian (LG), Hermite-Gaussian (HG), and spiral ones. Note that helical LG beam is a well-known example of optical vortex playing a relevant role in many areas ranging from optical tweezers to quantum optics [15]−[17]. The spiral beams, given as an appropriate superposition of the LG ones, have attracted the attention of researchers in last years due to the rotation of their intensity distribution around the optical axis during propagation [18]−[20]. Finally, in section 4, the characterization method is used for the beams generated by analogue holograms. The work ends with concluding remarks.

2. Phase retrieval approach based on measurement of WD projections

Phase retrieval has a relevant role in science and engineering. There exist various non-interferometric techniques for this task. Most of them, either iterative or non-iterative ones, involve digital post processing. In particular, the phase information can be recovered using non-iterative approaches based on so-called transport of intensity equation [21]−[24]. Nevertheless, it is often mathematically complex (e.g. specifying correct boundary conditions for

#140087 - $15.00 USD Received 22 Dec 2010; revised 20 Feb 2011; accepted 23 Feb 2011; published 17 Mar 2011

solving the equation) and it has important limitations in the experimental realization as for example: the image alignment as well as defocus calibration. Another well-established method is the Gerchberg-Saxton (GS) iterative algorithm [25]. It is widely used in different optical applications and permits to retrieve the input phase from the known amplitude (square root of intensity) distributions of the propagating beam, in Fraunhofer or Fresnel diffraction domains [25, 26]. These amplitudes play the role of constraint images. However, the main problem of the GS algorithm for the phase retrieval is the phase ambiguity resulting from converging to local minima solutions, which yields incorrect phase distribution. This issue is crucial in the case of noisy constraint images that are often found in experimental measurements. There exist several proposals to solve this problem by using statistical methods [27], but they demand a great amount of computational resources. The main idea to reduce phase ambiguity and speed up the algorithm convergence is acquiring more information about the beam by increasing the number of constraints [26] and by varying their type [8, 28]. For example the introduction of astigmatism in the optical setup, used for constraint image generation, solves certain problems in the phase recovery for the case of stable modes. In particular, it permits to determine the direction of phase rotation of helical Laguerre-Gaussian beams [28].

Here we briefly explain an iterative phase retrieval approach based on the GS algorithm that takes advantage of the controlled astigmatism, which can be produced by using a cylindrical lens with variable focal length given by the transmittance function

$$L_j(x,y) = \exp\left(-i\pi\frac{(x\cos\theta + y\sin\theta)^2}{\lambda \mathrm{f}_j}\right), \tag{1}$$

where λ is the wavelength, θ is the rotation angle that defines the lens orientation in the transversal plane, f_j is the focal length and j is an integer. The input beam $f(x,y)$ passes through the lens, Eq. (1), and then propagates a distance z. Considering the Fresnel diffraction regime, the outgoing beam $f_{out}(\mathbf{r}_o) = \mathrm{F}_z[f(\mathbf{r}_i)L_j(\mathbf{r}_i)](\mathbf{r}_o)$ is given by

$$f_{out}(\mathbf{r}_o) = \frac{\exp(i2\pi z/\lambda)}{i\lambda z}\iint f(\mathbf{r}_i)L_j(\mathbf{r}_i)\exp\left(i\pi\frac{(x_o-x_i)^2+(y_o-y_i)^2}{\lambda z}\right)\mathrm{d}\mathbf{r}_i, \tag{2}$$

where $\mathbf{r}_{i,o} = (x_{i,o}, y_{i,o})$ are the input and output spatial coordinates. The square root of the intensity distribution that coincides with the scaled WD projection, $|f_{out}(\mathbf{r}_o)|$, is used as constraint image. In our case the propagation distance z is fixed and the beam transformation is only performed by varying the focal length as $\mathrm{f}_j = \alpha_j z$. This fact results in a robust and flexible optical setup because it avoids axial movements of the optical elements. The phase distribution of the input beam can be numerically retrieved using the constraint images corresponding to different values of the focal length. To obtain an appropriate scale and sampling of the constraint image, at the measurement plane, the parameters z and α_j have to be chosen according to wavelength, input image size and detector dimensions (e.g. CCD chip). In particular, we consider a convergent cylindrical lens ($\alpha_j > 0$) with $\theta = \pi/4$.

Let us now describe the iterative algorithm whose flow chart is depicted in Fig. 1. The amplitude (modulus) of the input signal is denoted as $E_0 = |f(x,y)|$, whereas $E_j = \left|\mathrm{F}_z[f(x,y)L_j(x,y)]\right|$ is the amplitude of the constraint image, where $j = 1, 2, ..., M$ (M constraint images) and $L_j(x,y)$ is the phase modulation of the cylindrical lens with focal length f_j. The retrieved phase distribution $\phi_{k,M}(x,y)$ at each loop $k = 1, 2, ..., N$ is obtained as it follows:

1. Calculate free-space propagation at distance z of the complex field $S_k(x,y) = E_0\exp(i\phi_{k,j})$ modulated by the lens function $L_j(x,y)$. A constant or random phase can be used as $\phi_{1,1}$;

#140087 - $15.00 USD Received 22 Dec 2010; revised 20 Feb 2011; accepted 23 Feb 2011; published 17 Mar 2011

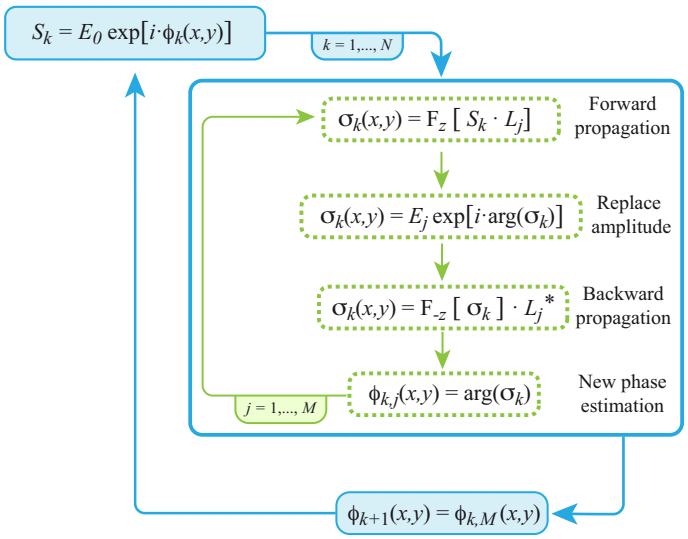

Fig. 1. Flow chart of the proposed phase retrieval algorithm.

2. Replace the resulting amplitude by the constraint image E_j found from the intensity distribution measured at z;

3. Calculate the back-propagation at distance $-z$ of the obtained complex field, and modulate the resulting field by the conjugate transmittance function of the lens $L_j^*(x,y)$;

4. The estimated phase $\phi_{k,j+1}(x,y)$ is used as initial one for the next iteration $j+1$.

The phase estimation $\phi_{k,M}(x,y)$ calculated after $j = M$ iterations is used for the next loop $k+1$, in which all constraint images are again used for steps i − iv). The algorithm ends at $k = N$ when the convergence is reached. Therefore the total number of iterations is $N \times M$.

Let us illustrate this phase retrieval method on the example of the Laguerre−Gaussian (LG) mode given by

$$\mathrm{LG}_{p,l}^{\pm}(\mathbf{r};w) = w^{-1}\left(\frac{p!}{(p+l)!}\right)^{1/2}\left(\sqrt{2\pi}\frac{x \pm iy}{w}\right)^{l}\mathscr{L}_p^l\left(\frac{2\pi}{w^2}r^2\right)\exp\left(-\frac{\pi}{w^2}r^2\right), \qquad (3)$$

where: $r^2 = x^2 + y^2$, w is the beam waist, and $\mathscr{L}_p^l$ is the Laguerre polynomial with radial index p and azimuthal index l.

In particular, we study the $\mathrm{LG}_{2,4}^{+}$ input beam displayed in Fig. 2(a). Beam waist is set at $w = \sqrt{\lambda z}$, where the wavelength $\lambda = 532$ nm and the propagation distance $z = 0.4$ m correspond to our experimental setup described in section 3. Retrieved phases obtained after $N \times M = 96$ iterations using $M = 1, 2, 3$ and 4 constraint images, are shown in Fig. 2(b). The relative root mean square (RMS) error of the retrieved phase, corresponding to each iteration, is given by

$$\mathrm{RMS}(k,j) = \left(\iint \left|E_0 \exp(i\phi) - E_0 \exp\left(i\phi_{k,j}\right)\right|^2 \mathrm{d}\mathbf{r}\right)^{1/2} \times \left(\iint \left|E_0 \exp(i\phi)\right|^2 \mathrm{d}\mathbf{r}\right)^{-1/2}, \qquad (4)$$

where ϕ is the phase of the test signal ($\mathrm{LG}_{2,4}^{+}$), see Fig. 2(c). These results demonstrate that the increase of the number M of constraint images speeds up the convergence of the RMS error. Convergence in the phase retrieval is reached at $N \times M = 96$ iterations with a RMS value of 0.02

#140087 - $15.00 USD Received 22 Dec 2010; revised 20 Feb 2011; accepted 23 Feb 2011; published 17 Mar 2011

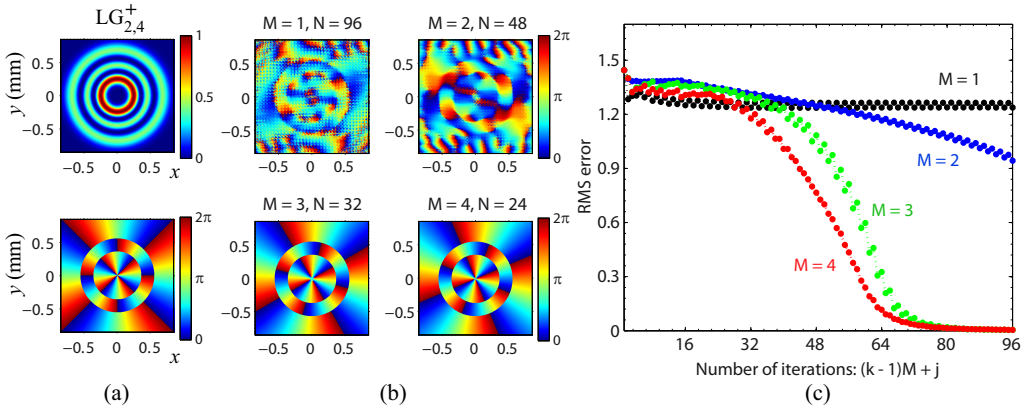

Fig. 2. (a) Intensity and phase distributions of the $LG^{+}_{2,4}$ beam. (b) Phase distribution retrieved after $N \times M = 96$ iterations using several constraint images M. (c) Evolution of the RMS error as a function of the number of iterations and constraint images. RMS values after $N \times M = 96$ are: 1.23 ($M = 1$), 0.94 ($M = 2$), 0.02 ($M = 3$), and 10^{-5} ($M = 4$).

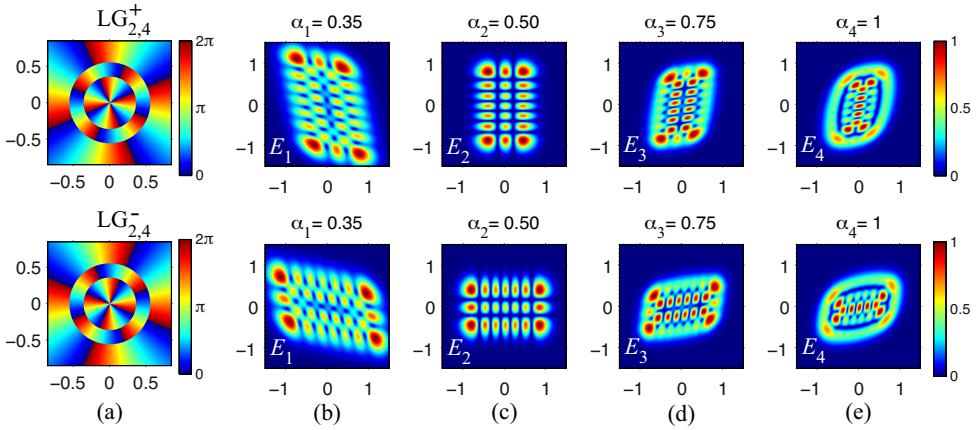

Fig. 3. (a) Retrieved phase associated to the $LG^{+}_{2,4}$ and $LG^{-}_{2,4}$ beams, obtained using $N \times M = 96$ iterations and $M = 4$ constraint images (RMS 10^{-5}). (b)-(e) The four constraint images (E_j) corresponding to each LG beam, displayed at first and second rows respectively.

and 10^{-5} for $M = 3$ and $M = 4$, respectively. We conclude that at least three constraint images are required to obtain good phase recovery using a low number of iterations. The numerical calculation was preformed with 1024×1024 points. Each constraint image E_j is associated with a single value of the focal length given as $f_j = \alpha_j z$, where: $\alpha_1 = 0.35$, $\alpha_2 = 0.5$, $\alpha_3 = 0.75$ and $\alpha_4 = 1$.

Notice that the beam propagation through an isotropic system does not allow distinguishing a stable mode from its complex conjugated [8]. However, by adding a controlled astigmatism it is possible to do this, as it is displayed in Fig. 3 for the example of $LG^{+}_{2,4}$ and $LG^{-}_{2,4}$ modes: the corresponding constraint images present a relative rotation of $\pi/2$ and a reflection. It is expected that the noise depending error in the phase estimation is also reduced by using several constraint images as reported in [28]. In the next sections we experimentally demonstrate the

#140087 - $15.00 USD Received 22 Dec 2010; revised 20 Feb 2011; accepted 23 Feb 2011; published 17 Mar 2011

robustness of the proposed approach against additive noise.

Finally, we stress that the Fast Fourier Transform (FFT) can be used for accurate numerical calculation of the Fresnel diffraction integral, Eq. (2), see for example [29]. It has been proved in several examples mentioned below that the algorithm typically converges within 1 minute (GNU/Linux workstation, Intel Core i7 processor, Matlab R2010a) after $N \times M = 96$ iterations, where $M = 4$ is the number of constraint images of 1024×1024 pixels. Convergence time can be optimized using a faster programming language. These facts make the described method a versatile tool for beam characterization, as it will be shown in the next section. We underline that, in our case, the cylindrical lens is implemented by means of the SLM. Nevertheless, conventional glass cylindrical lenses can be used as well.

3. Generation of arbitrary paraxial beams via CGH and their optical characterization

3.1. Design of CGH for beam generation

It is well-known [4] that an arbitrary scalar complex field described by

$$f(x,y) = a(x,y)\exp\left[i\phi(x,y)\right], \tag{5}$$

where $a(x,y)$ and $\phi(x,y)$ are the amplitude and phase distribution respectively, can be encoded as a phase CGH with a transmittance function

$$H(x,y) = \exp\left[i\psi(a,\phi)\right]. \tag{6}$$

The encoding phase $\psi(a,\phi)$ can be found representing $H(x,y)$ as a Fourier series in the domain of $\phi(x,y)$. For instance, in [6] it is demonstrated that $f(x,y)$ is recovered from the first-order term of such Fourier expansion by using the following hologram phase modulation function:

$$\psi(a,\phi) = g(a)\sin\phi, \tag{7}$$

if the condition $J_1\left[g(a)\right] = a$, is fulfilled for every value of the normalized amplitude $a(x,y) \in [0,\,1]$, where $J_1(\rho)$ is the Bessel function of first order. Inverting the latter relation the function $g(a)$ is defined, see [6] for further details. There exists another encoding approach, reported in [5], with hologram phase modulation:

$$\psi(a,\phi) = g(a)\phi, \tag{8}$$

and inversion condition $\mathrm{sinc}\left[1-g(a)\right] = a$, where $\mathrm{sinc}\left(\rho\right) = \sin\left(\pi\rho\right)/\pi\rho$. Both types of CGHs are useful for the generation of arbitrary beams as demonstrated in [6] and [30]. We underline that other types of CGHs studied in [4, 6, 31] are limited because they require the design of an specific aperture for each signal, and therefore they are less versatile. To isolate the encoded field $f(x,y)$ from other terms of the Fourier expansion, a carrier phase $\varphi_c = 2\pi(u_0 x + v_0 y)$ is added to the modulation function: $\psi(a,\phi+\varphi_c) \bmod 2\pi$. The further spatial filtering, that can be optically performed using a 4-f telescopic system, permits to select the corresponding term according to the value of spatial frequencies (u_0, v_0).

To estimate the quality of the experimentally generated beam, it is usual to compare its intensity distribution measured at the image plane with the theoretical one [6, 31, 32]. However, this information is not complete because the phase is not taken into account. In this work we propose a beam characterization technique to analyze both the intensity and phase distributions, which fully describe the beam propagation. For phase retrieval the iterative technique discussed in the previous section is used. The quality of a beam synthesized by CGH depends not only on the encoding method but also on the properties of the SLM and the entire optical setup used for the field generation. As we will show in the next section 3.2, the same phase retrieval technique

#140087 - $15.00 USD Received 22 Dec 2010; revised 20 Feb 2011; accepted 23 Feb 2011; published 17 Mar 2011

can also be applied to detect aberrations of the optical system, which can be compensated during the hologram generation process. These adaptive CGHs increase the feasibility of the synthesized beams.

3.2. *Experimental setup and its optical characterization*

The scheme of a typical experimental optical setup used for beam generation via CGH is depicted in Fig. 4(a). A linearly polarized collimated beam is modulated by the CGH addressed into a SLM. In our case we use a Nd:YAG laser ($\lambda = 532$ nm), with output power of 300 mW and a reflective LCoS-SLM (Holoeye PLUTO, 8-bit gray-level, pixel pitch of $8\,\mu$m and 1920×1080 pixels) operating in phase-only modulation, which was calibrated for a 2π phase shift at $\lambda = 532$ nm. The LCoS display performance depends on the electrical signal scheme addressed to the SLM device. Such an electrical signal yields different polarimetric responses of the display as for example the phase-shift obtained [33]. In order to avoid efficiency degradation in beam generation due to high time fluctuations of the displayed phase, we implement the so-called "5-5(543)" electrical signal scheme provided by the SLM manufacturer that is not often set by default. This configuration gives better efficiency of the displayed phase even for phase-shift shorter than 2π, as demonstrated in [33]. An exhaustive study about LCoS's optical performance and its characterization can be found in [33, 34].

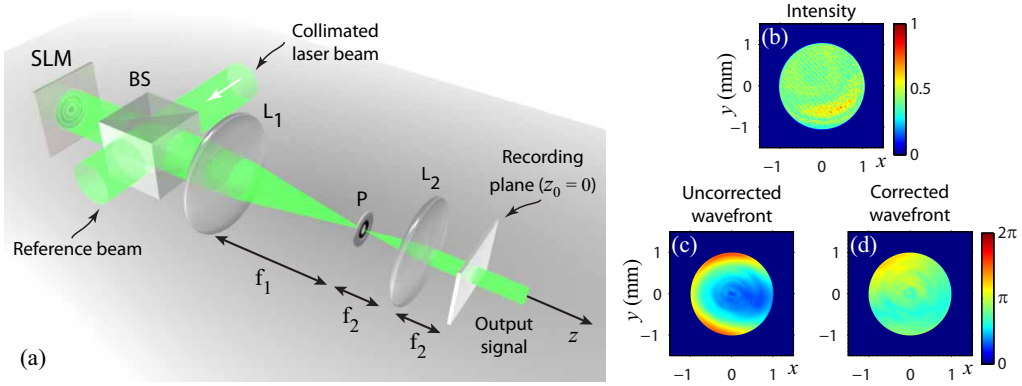

Fig. 4. (a) Experimental setup for generating arbitrary paraxial beams. The SLM displays a CGH associated to the complex signal to be generated. BS is a cube beam splitter, L_1 and L_2 are spherical relay lenses (with a diameter of 5.1 cm) working as telescope $0.4\times$, focal lengths: $f_1 = 25$ cm and $f_2 = 10$ cm, in our case. Pinhole P is located at Fourier plane of L_1 for spatial filtering. (b) SLM's area for CGH addressing, imaged at plane $z_0 = 0$. Retrieved phase $\phi_{ab}(x,y)$ of this region before (c) and after correction (d), see Table 1.

Spatial filtering is achieved at the Fourier plane of the spherical lens L_1, see Fig. 4(a), whereas the SLM is located at its back focal plane. Therefore the encoded beam $f(x,y)$ is generated at the imaging plane (at $z_0 = 0$) of the telescope, which corresponds to the focal plane of relay lens L_2, see Fig. 4(a). Telescope magnification was set at $0.4\times$. The intensity distribution of the outgoing beam is recorded by a CCD camera (Spiricon SP620U, 12-bit gray-level, pixel pitch of $4.4\,\mu$m and 1620×1200 pixels), which is placed at distance $z = 0.4$ m for acquiring of constraint images.

First, we apply the proposed phase retrieval approach for the calibration of the setup. As test signal $f(x,y)$, we consider a circular pupil with radius $r_0 = 2.5$ mm (function $\mathrm{circ}(r/r_0)$), associated to the region of the SLM display further used for the CGH implementation. Notice that this region is imaged with scale $0.4\times$ at plane $z_0 = 0$, see Fig. 4(b) where the intensity

#140087 - $15.00 USD Received 22 Dec 2010; revised 20 Feb 2011; accepted 23 Feb 2011; published 17 Mar 2011

distribution is shown. The corresponding phase distribution $\phi_{ab}(x,y)$ at plane $z_0 = 0$ is displayed in Fig. 4(c), which was retrieved using eight constraint images (registered at $z = 0.4$ m) and $N \times M = 288$ iterations. We considered such a number of constraint images and iterations in order to reduce phase ambiguity arising from noisy measurements. In this case the cylindrical lens, see Eq. (1), addressed into the SLM was set with focal lengths $f_j = \alpha_j z/s^2$, where $z = 0.4$ m, $s = 0.4$ is the telescope-scaling factor, and $\alpha = 0.35, 0.5, 0.75, 1, 1.25, 1.5, 1.75, 3.5$.

The wavefront distortion $\phi_{ab}(x,y)$ is caused by static aberrations arising from the whole optical setup: SLM, relay lenses, collimation of the beam, etc. To analyze this aberration, $\phi_{ab}(x,y)$ is decomposed in terms of Zernike's orthogonal polynomials. We used the first 40 coefficients as defined in [10, 35]. Table 1 displays the most significant terms, showing that for the distorted wavefront the astigmatism and spherical aberration are predominant. These large distortion values are present in other reflective LCoS SLMs, see [11, 12, 14]. Fortunately, the aberration can be compensated by addressing its conjugated phase, $-\phi_{ab}(x,y)$, into the SLM. After this correction the resulting wavefront presents Zernike coefficients bellow $\lambda/16$ except for astigmatism at 45° ($\simeq -\lambda/8$) and third-order spherical aberration ($-\lambda/5$), see Table 1. These results are similar to the ones previously reported for other LCoS devices by using a Shack-Hartmann (SH) wavefront sensor for its characterization, see [14] and references cited therein. It is expected to improve this wavefront correction by repeating the latter procedure several times, by increasing the number of constraint images, or by performing further calibration of the phase modulation response of such SLM devices, as reported in [33]. For example, it is demonstrated in [14] that after nine iterative phase corrections based on the SH sensor measurements all Zernike's coefficients, listed in Table 1, are below $\lambda/20$. In the latter work, it is shown that the flatness deviation of the SLM (Holoeye LCR-2500, 8-bit gray-level, pixel pitch of $19\,\mu$m) is compensated from 0.8λ to $\lambda/16$ RMS for its central area of about 3 mm in diameter. In our case the wavefront flatness is compensated up to $\lambda/13$ and $\lambda/15$ RMS for a circular area of 5 mm and 3 mm in diameter, respectively. Notice that both SLM devices are similar except for the spatial resolution. The proposed approach also allows characterizing the generated beam, as it will be studied in the next sections.

Table 1. Zernike Coefficients (waves at 532 nm) of Uncorrected and Corrected Wavefront

Zernike Term−Aberration	Before correction	After correction
Defocus	1.24	−0.02
Astigmatism at 0°	−0.31	0.06
Astigmatism at 45°	−1.30	−0.13
Coma at x	0.09	−0.04
Coma at y	−0.12	−0.02
3rd order spherical	−0.28	−0.20
Trefoil at 0°	0.01	0.01
Trefoil at 45°	−0.11	0.02
5th order astigmatism at 0°	0.01	−0.03
5th order astigmatism at 45°	0.10	−0.02

3.3. Characterization of the generated beams

First we analyze the quality of the CGH-type 1 and 2 associated to Eq. (7) and Eq. (8), respectively. As input signals we now consider LG modes given by Eq. (3) and HG modes written as

$$\mathrm{HG}_{m,n}(\mathbf{r};w) = \mathscr{H}_m\left(\sqrt{2\pi}\frac{x}{w}\right)\mathscr{H}_n\left(\sqrt{2\pi}\frac{y}{w}\right)\exp\left(-\frac{\pi}{w^2}r^2\right), \tag{9}$$

#140087 - $15.00 USD Received 22 Dec 2010; revised 20 Feb 2011; accepted 23 Feb 2011; published 17 Mar 2011

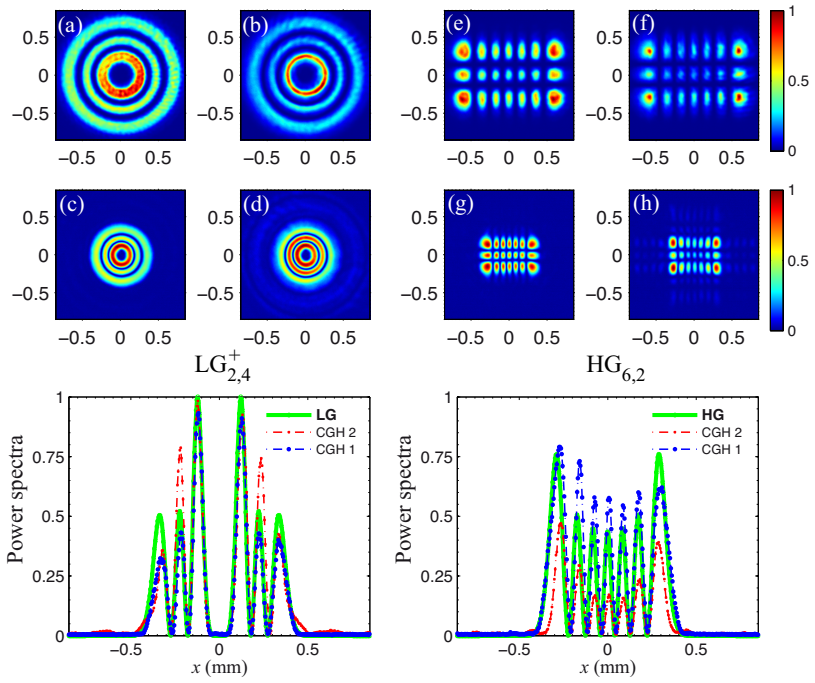

Fig. 5. Experimental results. Intensity of the $LG^{+}_{2,4}$ beam generated by means of CGH−type 1 (a) and 2 (b). Fourier spectra of these beams are shown in (c) and (d), correspondingly. The $HG_{6,2}$ generated by CGH−type 1 (e) and 2 (f) and their power spectra (g) and (h), respectively. The third row displays the power spectra profile, along x axis, corresponding to (c, d) and (g, h): theoretical profile (green line) and the measured ones associated to CGH−type 1 (blue line) and 2 (red line).

where $\mathscr{H}_m$ is the Hermite polynomial. Both types of beams have phase singularities, helical or binary phase structure, that make difficult the phase retrieval. In particular the $LG^{+}_{2,4}$ and $HG_{6,2}$ modes are studied. We remind that the adaptive phase hologram (ACGH) addressed into the SLM is $\psi(a, \phi - \phi_{ab} + \varphi_c)$, where: ϕ is the phase of the input signal, ϕ_{ab} is the phase distortion of the setup [shown in Fig. 4(c)] used for the wavefront correction, and φ_c is the linear carrier which spatial frequency is set as $u_0 = v_0 = 1/4d$ in our case (d is the SLM's pixel pitch). A fast and useful way to visualize the beam-quality degradation due to the residual phase distortion, obtained after the wavefront correction [see third column of Table 1], consists of analyzing the power spectrum of the generated beam. Notice that the form of the power spectrum for the studied beam is identical to its intensity distribution except from a scaling factor. This test can be carried out using a convergent spherical lens. Figure 5 shows the generated beam at the image plane ($z_0 = 0$) and its power spectrum obtained at the focal plane of a spherical lens (focal length of 20 cm, N-BK7 glass). There exists a small amount of distortion due to the residual aberration of the setup previously characterized. Moreover, in the case of CGH-type 2 it is observed a significant mismatch with the theoretical intensity distribution at image plane as well as the Fourier plane. It is known that CGH-type 2 reconstructs a beam corrupted by noise distortions arising from high-order diffractions terms, as it was previously demonstrated in [6] by numerical simulation. While the beams generated by CGH-type 1 do not present this problem. Therefore, we conclude that encoding CGH-type 1 is more accurate for beam generation in our experimental setup.

#140087 - $15.00 USD Received 22 Dec 2010; revised 20 Feb 2011; accepted 23 Feb 2011; published 17 Mar 2011

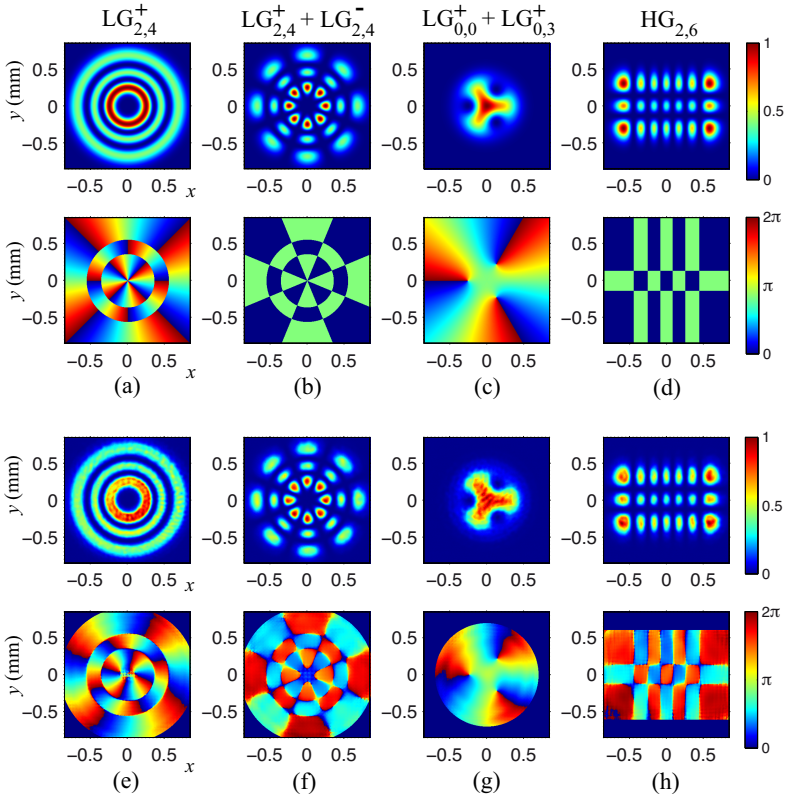

Fig. 6. Intensity and phase distributions of the $LG^{+}_{2,4}$ (a), $LG^{+}_{2,4}+LG^{-}_{2,4}$ (b), spiral beam $LG^{+}_{0,0}+LG^{+}_{0,3}$ (c), and $HG_{6,2}$ (d) mode, displayed at the first and second rows correspondingly. (e)-(h) Experimental results: intensity of the generated beam and its phase distribution reconstructed using $M=8$ constraint images and $N\times M=288$ iterations.

To evaluate the quality of the generation of several types of beams, displayed in Fig. 6(a)−6(d), we apply the phase retrieval approach previously discussed. The intensity distribution of the generated beams at the image plane ($z_0=0$) are shown in Fig. 6(e)−6(h) as well as the corresponding retrieved phase distributions. For each case we used the same values of the transformation parameter α, $M=8$ constraint images and $N\times M=288$ iterations. These experimental results are in good agreement with the theoretical ones displayed in Fig. 6(a)−6(d). We underline that the constraint images are measured after implementing the corresponding phase hologram $\psi(a,\phi-\phi_{ab}+\varphi_c+\arg\{L_j\})$, where ϕ is the encoded beam's phase and $\arg\{L_j\}$ is the phase function associated to the cylindrical lens with focal length $f_j=\alpha_j z/s^2$.

The global beam quality can be quantitatively evaluated by means of the Signal to Noise Ratio (SNR) given by [36]

$$\mathrm{SNR} \quad = \quad \iint |f(\mathbf{r})|^2\,\mathrm{d}\mathbf{r}\times\left(\iint |f(\mathbf{r})-\beta s_e(\mathbf{r})|^2\,\mathrm{d}\mathbf{r}\right)^{-1}, \tag{10}$$

where

$$\beta=\iint \Re\{f(\mathbf{r})s_e^*(\mathbf{r})\}\,\mathrm{d}\mathbf{r}\times\left(\iint |s_e(\mathbf{r})|^2\,\mathrm{d}\mathbf{r}\right)^{-1}, \tag{11}$$

#140087 - $15.00 USD Received 22 Dec 2010; revised 20 Feb 2011; accepted 23 Feb 2011; published 17 Mar 2011

is a constant normalization factor for the power of the signal $s_e(\mathbf{r})$ under evaluation and $\Re$ denotes the real part of the signal. This definition is appropriate for beam characterization because it permits a quality estimation of both the intensity and phase distribution. For the reconstructed beams shown in Fig. 6(e)−6(h) a SNR value (given in decibels) about 12 dB is obtained. In this SNR calculation the defocus and tilt aberrations have been neglected because they yield small amount of uniform scaling and shift in the beam along its propagation. Notice that the beam quality is often estimated using the SNR of the intensity distribution, which is about 20 dB in our case. As can be seen, such an estimation of the beam quality artificially yields higher SNR value because noise in beam's phase is not considered. In spite of the residual phase distortion arising from the optical setup, the generated beam shows high stability under free-space propagation as expected. In Fig. 7 some of the measured constraint images for the case of $\mathrm{LG}^{+}_{2,4}$ mode are displayed. These results also demonstrate a good agreement with the theoretical ones shown in Fig. 3, and therefore confirm that the residual wavefront distortion does not significantly decrease the quality of the beam.

It is also possible to estimate the beam quality by calculating the beam purity as defined in [37]. The beam purity η is given as an inner product of the encoded signal $f(\mathbf{r})$ and the output signal $s_e(\mathbf{r})$ under evaluation as it follows

$$\eta = \left| \iint f^{*}(\mathbf{r}) \beta s_e(\mathbf{r}) \mathrm{d}\mathbf{r} \right|^2 , \tag{12}$$

where $*$ denotes the complex conjugate. Notice that the signals are normalized using the parameter β and the ideal purity is $\eta = 1$. In our case the beam purity is about $\eta = 0.88$ for the beams displayed in Fig. 6(e)−6(h). This result reasonably agrees with the theoretical one $\eta = 0.97$ estimated in [32] by means of the numerical simulation of a practical SLM and the corresponding CGH-encoding approach, which does not take into account the aberrations of the optical setup. The estimation of the beam purity was also experimentally studied in [31] by analyzing the correlation between the intensity distributions of the measured and theoretical modes. Nevertheless, it does not give a quantitative estimation of η because such a correlation generally varies during beam propagation while η does not, as discussed in [31]. In contrast, the proposed approach allows experimentally performing a quantitative estimation of the beam purity η as well as the beam quality SNR for paraxial beams. While the considered quality parameters are important for global beam characterization, the direct comparison between the phase and amplitude distributions of the encoded and generated beams provides detailed information. Thus, the estimated Zernike coefficients of the residual wavefront indicate the way of possible improvement of the beam generation.

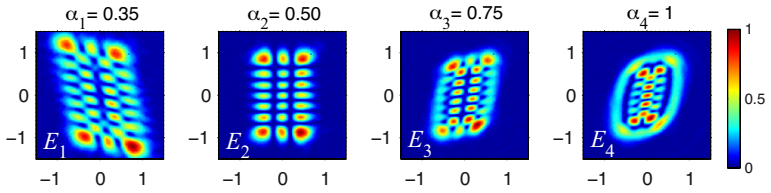

Fig. 7. Experimental results. Measured constraint images E_j (square root of intensity distribution) associated to $\mathrm{LG}^{+}_{2,4}$ mode.

4. Quality control of beams recorded onto a holographic storage medium

Finally, we apply the proposed method for the analysis of the quality of the beams recorded onto holographic storage medium. As an example of recording material, a highly efficient pho-

#140087 - $15.00 USD Received 22 Dec 2010; revised 20 Feb 2011; accepted 23 Feb 2011; published 17 Mar 2011

topolymerizable glass developed by us [38] is used. This holographic material exhibits high optical performance for continuous as well as femtosecond laser applications [39]. The interferogram between the $LG^{+}_{2,4}$ beam [Fig. 6(e)], generated by the previously described method, and a collimated reference beam is recorded onto this material. In our case the reference beam is redirected towards the recording plane (placed at $z_0 = 0$, see Fig. 4) in such a way that a volume phase hologram is registered (spatial frequency of 400 lines/mm and sample thickness is $80\,\mu$m). The hologram is reconstructed by illuminating with an appropriate reading beam (e.g. the reference beam). Figure 8(a) and 8(b) display the reconstructed hologram of the $LG^{+}_{2,4}$ mode and its power spectrum measured at the focal plane of the convergent spherical lens, respectively. Since the holographic material is sandwiched between two microscope coverslip glass there exists a small amount of distortion arising from its lack of flatness, as it is observed in Fig. 8(b).

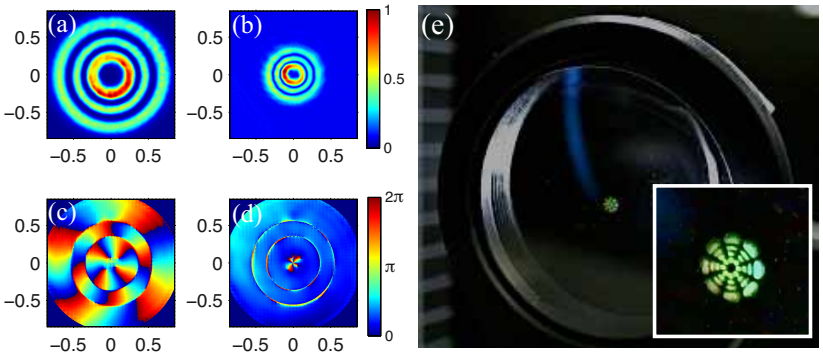

Fig. 8. Experimental results. (a) Holographically recorded $LG^{+}_{2,4}$ beam onto a photopolymerizable glass and its power spectrum (b). (c) Retrieved phase of the reconstructed beam and its wavefront distortion (d). (e) Reconstruction of $LG^{+}_{3,4} + LG^{-}_{3,4}$ beam recorded on a photopolymerizable glass, see Media 1.

To analyze such a distortion we again apply the proposed phase retrieval approach to the reconstructed beam, Fig. 8(a). In this case, to obtain the constraint image, the reading beam is generated by the SLM. Therefore the hologram is uniformly illuminated by a reading beam whose phase distribution corresponds to the cylindrical lens with focal length $f_j = \alpha_j z/s^2$. The constraint image is again measured at $z = 0.4$ m for each reading beam. Here we consider the same number of constraint images ($M = 8$), as previously studied. The retrieved phase is shown in Fig. 8(c). Since we analyze the beam reconstructed on the -1st diffraction order of the volume hologram, it corresponds to the $LG^{-}_{2,4}$ mode which is the complex conjugated of the recorded (object) beam $LG^{+}_{2,4}$. The residual wavefront distortion obtained after the comparison with the theoretical phase of the $LG^{-}_{2,4}$ mode is displayed in Fig. 8(d). These results confirm a good agreement between the reconstructed and object beams. Such a distortion presents a predominant increment of 0.11λ and 0.15λ for coma at x and y, and 0.07λ for astigmatism at 0° with respect to the residual one of the optical setup characterized in section 3. It is mainly caused by the lack of flatness of the coverslip glass attached to the holographic material and causes a small decrease in the beam quality, SNR is about 10 dB and beam purity is $\eta = 0.84$. In order to minimize this distortion a glass wafer with lower RMS flatness deviation can be used instead of the microscope coverslip glass, which in our case was mounted into a lens holder with an aperture diameter of 2.54 cm [see Fig. 8(e)]. Nevertheless, the experimental results are in good agreement with the theoretical predictions.

#140087 - $15.00 USD Received 22 Dec 2010; revised 20 Feb 2011; accepted 23 Feb 2011; published 17 Mar 2011

The considered analogue holograms can be applied in many optical setups providing their compactness. Moreover, the high optical performance (diffraction efficiency is about 90%) and damage threshold of this holographic material [38, 39] makes them very useful for optical trapping, ultrafast optics, photonics, etc. To illustrate the hologram performance, in Fig. 8(e) the hologram of a $LG^{+}_{3,4} + LG^{-}_{3,4}$ beam is shown, see also Media 1.

5. Conclusions

A robust and versatile technique for the characterization of holographically-synthesized beams based on iterative phase retrieval from several WD projections has been established. The recovered phase distribution allows estimating the global parameters of the beam generation quality, such as SNR and the beam purity. Moreover, the analysis of the wavefront distortion −the difference between the phase distributions of the encoded and generated signal − applying the Zernike polynomials decomposition determines the static aberrations arising from the used optical setup as well as the ones introduced by the hologram encoding method. Based on this information significant improvements in the process of beam generation can be incorporated.

The proposed method have been applied for the characterization of the optical setup (further required for the hologram implementation) and for the analysis of the quality of beams generated by digital and analogue holograms. It has been demonstrated that the beam quality degradation is mainly caused by aberrations arising from the SLM, which can be detected using the proposed approach. Thus, the flatness deviation of the SLM has been compensated up to $\lambda/15$ RMS leading to significantly improvement of beam quality: a SNR value about 12 dB and beam purity $\eta = 0.88$ are obtained. These previously characterized beams have been recorded onto a highly efficient photopolymerizable material. The analysis of the beam reconstructed from the analogue hologram presents small amount of additional (compared with the object beam) wavefront distortion caused by the flatness deviation of the glass wafer covering the holographic material. In this case a SNR value of 10 dB and $\eta = 0.84$ are obtained. The high optical throughput of these analogue holograms make them attractive for different applications such as optical information processing, ultrafast optics, photonics, microparticle manipulation, etc.

Acknowledgments

The financial support of the Spanish Ministry of Science and Innovation under project TEC2008-04105 is acknowledged. José A. Rodrigo gratefully thanks a “Juan de la Cierva” grant and A. Cámara acknowledges the financial support of the “Comunidad de Madrid” and the European Social Fund.

#140087 - $15.00 USD Received 22 Dec 2010; revised 20 Feb 2011; accepted 23 Feb 2011; published 17 Mar 2011